

Vision-Based Range Regulation of a Leader-Follower Formation

Patricio Vela, Amir Betser, James Malcolm, and Allen Tannenbaum

Abstract—This brief describes a single-vehicle tracking algorithm relying on active contours for target extraction and an extended Kalman filter for relative position estimation. The primary difficulty lies in the estimation and regulation of range using monocular vision. The work represents a first step towards treating the problem of the control of several unmanned vehicles flying in formation using only local visual information. In particular, allowing only onboard passive sensing of the external environment, we seek to study the achievable closed-loop performance under this model.

Index Terms—Active contours, active vision, range-estimation, vehicle tracking.

I. INTRODUCTION

THIS BRIEF utilizes geometric active contours and Kalman filtering for the visual segmentation and tracking of flying vehicles. Tracking is a basic control problem whereby a system's output is to follow or track a reference signal, or equivalently a system's *tracking error* should be as small as possible relative to some well-defined criterion (say energy, power, peak value, etc.). The problem of visual tracking differs from standard tracking problems in that the feedback signal is not directly measured by the imaging sensors proper. The true measurements must be extracted via computer vision algorithms and interpreted by a reasoning algorithm before being used in the control loop. Within the context of vehicle tracking and regulation of leader-follower formations, the follower must be able to maintain a specific relative positioning between itself and the target. Line of sight angle is readily computable from the image itself and is used to infer the relative vector direction to the target. Range, on the other hand, is not generically observable from the image sequence alone; additional motion commands and processing are required to estimate range [1], [2]. This brief describes an extension to [1] for range-regulation.

The problem we consider here is the tracking of a leading unmanned vehicle (UV) *the Leader*, by another UV *the Follower*, without communication between the two vehicles. For the moment, we are considering planar motion only in order to assess how vision-based measurements can be used to improve an existing non-vision-based method. Sensing, for the Follower, is accomplished completely onboard and is passive. Such a problem

Manuscript received September 19, 2007; revised July 9, 2007. Manuscript received in final form May 15, 2008. Recommended by Associate Editor C.-Y. Su. This work was supported by Grants from AFOSR-MURI, AFOSR F49620-01-1-0017, MRI-HEL, and the National Science Foundation.

P. Vela, J. Malcolm, and A. Tannenbaum are with the School of Electrical and Computer Engineering, Georgia Institute of Technology, Atlanta, GA 30332-0250 USA (e-mail: pvela@ece.gatech.edu).

A. Betser was with the School of Electrical and Computer Engineering, Georgia Institute of Technology, Atlanta, GA 30332-0250 USA. He is now with Rafael, 31021 Haifa, Israel.

Color versions of one or more of the figures in this brief are available online at <http://ieeexplore.ieee.org>.

Digital Object Identifier 10.1109/TCST.2008.2000979

is considered in Sattigeri *et al.* [3], however, the authors rely on the existence of relative range measurements, which are not immediately available in the problem we wish to solve. Consequently, vision-based estimation of the relative range will be introduced.

1) *Related Work*: The majority of vision-based techniques for range or depth estimation result in dense range-maps. Dense range-maps may be estimated using optical flow [4], [5] or optical differentiation [6]. Harding and Lane [7] compute depth by solving the inverse image projection using multiple views. A Minimum Descriptor Length approach to optical flow computation and range estimation is given in [8]. PDE based methods for solving the range problem can be found in [9]. Another approach couples a nonlinear observer with the tracking of various geometric objects (lines, curves, etc.) across multiple frames [10]. Murphey *et al.* [11] describe a “depth-finder” algorithm for planar motion. Many of these approaches are not real-time implementable or rely on static scenery. There are also geometric methods for tracking a coherent object across multiple frames for range estimation. Avidan and Shashua [2] utilize trajectory triangulation to solve for the relative range. Stein *et al.* [12] work out the geometry of vision for planar vehicles and compute the optimal sampling rate for estimation of range. These techniques are limited by model assumptions that need not hold in our case.

Much of the work regarding range estimation from bearings-only information is relevant to the problem at hand. The bearings-only problem deals with range estimation using passively obtained bearing data (typically from sonar). Huster and Rock [13] examine the real-time implementation of the extended Kalman filter found in [1]. This work was extended by Frew *et al.* within the context of optimal maneuvers for bearings-only target estimation and visual navigation [14], [15]. Other methods incorporate particle filters [16], multiple model hypotheses [17], or bias correction [18] to overcome the inherent limitations found in [1]. The limitations of bearings-only estimation can be traced to the paucity of sensor information regarding the external environment/target [19], [20], as does the need for persistent maneuvering of the follower [21]. Bearings-only target estimation cannot be used to regulate range as needed for a Leader-Follower scenario.

Using a visual sensor, information beyond target bearing is available. Recent efforts to fully incorporate the visual signal for achieving formation control can be found in [22]–[26]. Although the [26] incorporates additional information from the visual signal, the brief focuses on flocking and velocity heading consensus, as opposed to range-regulated formation control. While relevant, the other references incorporate additional knowledge in one of two ways: 1) through the use of a visual sensor that allows for direct estimation of range or 2) through inter-vehicle communication and centralized control. For the problem at hand, neither of these two options is available.

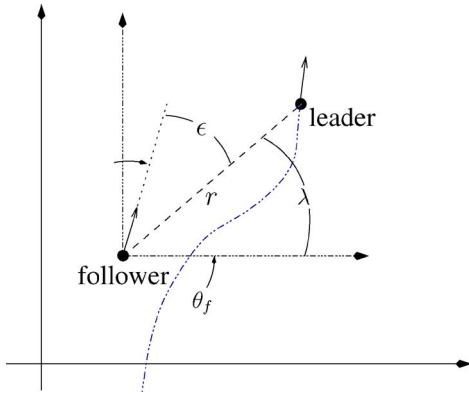


Fig. 1. Leader-Follower configuration.

2) *Contribution*: In the proposed vision-based range estimation implementation, additional image information is used to augment the standard bearings-only estimation process leading to an additional state in the estimation EKF when compared to the traditional bearings-only EKF. This brief focuses on proof-of-concept simulations implementing active contour tracking with the augmented EKF model for estimation of range and line of sight. Empirical analysis of the original versus the modified EKF exemplify the beneficial role of the visual sensor in the estimation process. The vision-based range estimator is an improvement over the standard bearings-only range estimator and also eliminates the need to follow an oscillatory trajectory. Furthermore, with the added vision-based estimation component, closed-loop formation regulation relative to a lead vehicle with piecewise constant velocity is achievable whereas it is not possible with bearings-only range estimation.

3) *Problem Formulation*: The problem consists of two planar UAVs, one of which is labelled the Leader and the other Follower. The Leader is following an unknown trajectory relative to which the Follower must track (c.f., Fig. 1). Available to the Follower are measurements of its own state (configuration, velocity, and acceleration) and the image obtained from a fixed, forward-pointing, onboard, monocular camera system.

The complete closed-loop system is summarized by the block diagram of Fig. 2. Of importance is the additional block for the vision sensor in the feedback loop. The image processing/computer vision block produces “measurements” (described in the sequel), which are sent to the Estimation block, itself implementing a Kalman filter strategy. The Estimation block calculates the relative range, the line of sight (LOS), and the LOS rate between the Leader and the Follower. These parameters are used by the Guidance block to produce the velocity and acceleration commands for the vehicle’s inner controller loop.

The measurement input to the Kalman filter are two angles. The first angle is the lead angle ϵ and the second is the maximum angle subtended by the Leader in the image plane α (depicted in Fig. 4 from the active contour tracking the Leader on the image plane.

4) *Organization*: This brief is decomposed into sections according to the bold blocks comprising the feedback loop in the block diagram of Fig. 2. The active contour algorithm for image segmentation is reviewed in Section II and its implementation

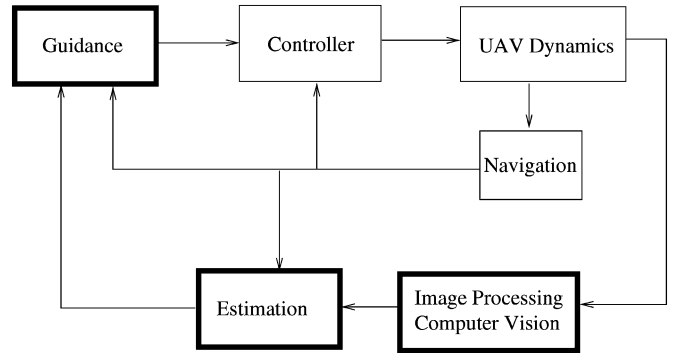


Fig. 2. System block diagram.

within the context of object tracking is discussed. Using the track signal provided by the active contour algorithm, Section III proposes an extended Kalman filter for range estimation. Once range is estimated and relative pose can be reconstructed, a controller is required to achieve the desired control objective. A simple, linear controller derived from missile guidance laws is described in Section IV. Finally, all of the elements are combined in Section IV-A with a Leader-Follower scenario whose resulting performance is analyzed.

II. OBJECT TRACKING VIA ACTIVE CONTOURS

The segmentation method for tracking the target relies on *snakes* or *active contours* [27], [28]. This section briefly discusses the active contour model chosen and how active contours conform to various object shapes and motions, making them ideal for segmentation, edge detection, shape modelling, and visual tracking. While there are a variety of alternative methods to arrive at target segmentations, in this brief, we use active contours to dynamically track a target and its shape across a sequence of images. The information extracted from the active contour process are the vision derived measurements.

In order to extract the target location and geometry from the image, an active contour algorithm tailored to the photometric properties of the imaged target should be chosen. Given that the target and background region have unique disjoint statistics, region-based active contours are effective solutions to the segmentation problem. The region-based active contour algorithm chosen is the Bayesian active contour method given in [29]. The algorithm assigns probability distributions to the interior and exterior regions and maximizes the integral of the negative log likelihood over the domain, as per

$$\begin{aligned} \mathcal{L} := & - \int_{\text{int}(\mathcal{C})} \log \mathcal{N}(I(x, y); \mu_{\text{in}}, \sigma_{\text{in}}) d\Omega \\ & - \int_{\Omega \setminus \text{int}(\mathcal{C})} \log \mathcal{N}(I(x, y); \mu_{\text{out}}, \sigma_{\text{out}}) d\Omega \end{aligned}$$

where \mathcal{C} describes the active contour defined over the planar domain Ω , \mathcal{N} represents a Gaussian distribution with parameters $\mu_{\text{in/out}}$ and $\sigma_{\text{in/out}}$, and $\text{int}(\mathcal{C})$ is the interior region of the



Fig. 3. Sample segmentation using active contour. The initial contour is the white dotted circle and the final contour is the white line surrounding the airplane.

curve. Applying the logarithm function to the Gaussian distributions leads to

$$\begin{aligned} \mathcal{L} := & \int_{\text{int}(\mathcal{C})} \left(\frac{1}{\sigma_{\text{in}}^2} (I(x, y) - \mu_{\text{in}})^2 + \log(\sqrt{2\pi}\sigma_{\text{in}}) \right) d\Omega \\ & + \int_{\Omega \setminus \text{int}(\mathcal{C})} \left(\frac{1}{\sigma_{\text{out}}^2} (I(x, y) - \mu_{\text{out}})^2 + \log(\sqrt{2\pi}\sigma_{\text{out}}) \right) d\Omega \end{aligned}$$

whose first variation is used to derive the gradient descent equations for the closed curve \mathcal{C}

$$\mathcal{C}_t = \frac{1}{\sigma_{\text{in}}^2} (I(x, y) - \mu_{\text{in}})^2 - \frac{1}{\sigma_{\text{out}}^2} (I(x, y) - \mu_{\text{out}})^2 + \log \left(\frac{\sigma_{\text{in}}}{\sigma_{\text{out}}} \right).$$

The method was shown to perform well even if the background did not precisely fit a Gaussian distribution so long as the foreground was well represented by a Gaussian. The extension to vector-valued imagery can be readily obtained from the previous equations [29]. Alternative distributions to a Gaussian can be chosen for more complex imagery.

There are fast implementations of these snake algorithms based on level set methods [30], [31]. The ability of snakes to change topology and quickly capture desired features makes them an indispensable tool for visual tracking algorithms [32]. Active contours derive the segmented data (as depicted in Fig. 3) that then drive the estimation process.

III. ESTIMATION PROCESS

In this section, we describe a modified algorithm for estimating the relative range r , LOS angle λ , and the LOS rate $\dot{\lambda}$ using the visual information obtained from a fixed, forward-pointing onboard camera. The algorithm is a modification of the extended Kalman Filter found in Aidala and Hammel [1]. The extended Kalman filter model equations involving relative range and LOS are

$$\dot{x}(t) = \begin{bmatrix} -2x_1(t)x_2(t) + x_4(t)a_N^{\text{LOS}}(t) \\ x_1^2(t) - x_2^2(t) + x_4(t)a_T^{\text{LOS}}(t) \\ x_1(t) \\ -x_2(t)x_4(t) \end{bmatrix} \quad (1)$$

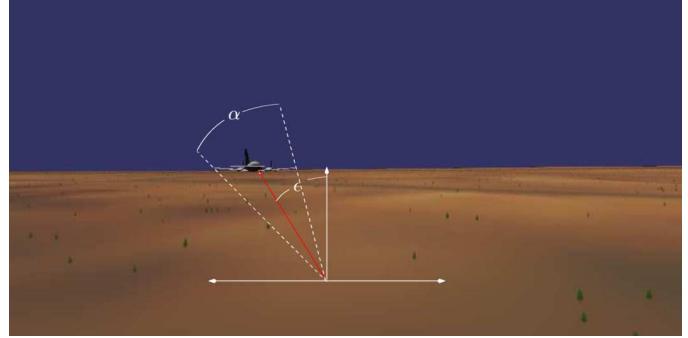


Fig. 4. Measurement inputs to Kalman filter as visualized in the simulation.

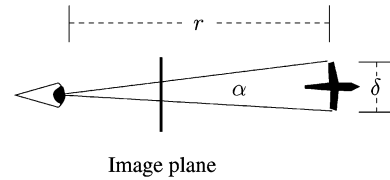


Fig. 5. Geometry of subtended angle.

with the filter states

$$x(t) = \begin{bmatrix} x_1(t) \\ x_2(t) \\ x_3(t) \\ x_4(t) \end{bmatrix} = \begin{bmatrix} \dot{\lambda} \\ \dot{r}/r \\ \lambda \\ 1/r \end{bmatrix} \quad (2)$$

where a_N^{LOS} and a_T^{LOS} are the relative acceleration normal and tangent to the LOS, respectively. The available measurement is the LOS angle as obtained from the lead angle ϵ , shown in Fig. 4

$$\lambda(t) = \theta_f(t) - \epsilon(t) + \omega_\lambda \quad (3)$$

where θ_f is the heading of the Follower, and ω_λ is measurement noise.

Aidala and Hammel demonstrated that the range state is unobservable except during certain Follower maneuvers [1]. Furthermore, should the Leader accelerate or maneuver in any way, the extended Kalman filter could diverge. Work has gone into understanding the optimal maneuvers for range estimation [33], and into extensions to the Kalman filter framework for overcoming the effects of Leader acceleration [17], [18].

1) *Extended Model*: The Kalman filter equations (1)–(3) do not completely utilize the information provided by an imaging camera. In particular, the captured image of the Leader provides indirect observation of the range through the equation

$$r = \frac{\delta}{2 \tan(\frac{1}{2}\alpha)} \quad (4)$$

where the parameter δ is the nominal length of the Leader, an unknown quantity (c.f. Fig. 5). This length is defined to be the longest axis of the plane (typically along the wing). By measuring the angle subtended by the Leader in the image plane α , the unobservable state r may be rendered observable during Follower motion. Consequently, adding the fifth state $x_5 \equiv \alpha$, with the dynamics

$$\dot{x}_5 = -x_2 \sin(x_5) \quad (5)$$

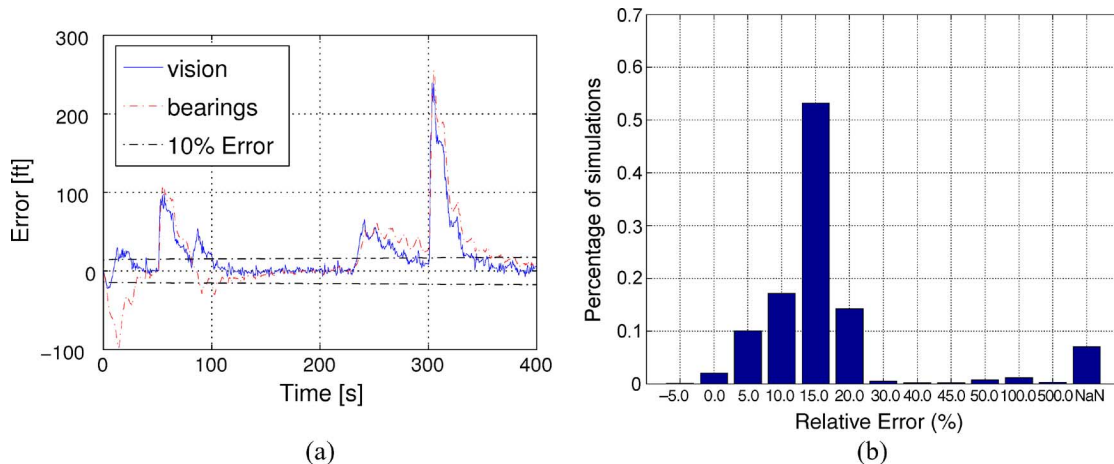


Fig. 6. Open-loop comparison of the Aidala and Hammel EKF to the proposed EKF with pointwise maneuvers of the lead aircraft. (a) Depicts a sample plot of the estimation error versus time and (b) shows the relative L_2 -norm error difference between the original and modified EKF algorithms as a percentage of 1000 simulations as a probability density. The NaN entry means that the Aidala and Hammel EKF failed to estimate; this happened for approximately 6% of the runs. The median performance difference for bearings-only EKF is 30% worse (assuming convergence occurs).

should improve the range estimates and provide a level of robustness to the estimation framework. This new state now provides range information during maneuvers tangent to the line of sight, whereas the original Kalman filter did not. Any acceleration by the Follower will provide range information to the Kalman filter.

Unfortunately, acceleration by the Leader still causes problems for the estimation process. Although the open-loop estimation process may suffer as a result, range limits introduced in the closed-loop system curtail the potential consequences. The range limits are obtained from (4) by assuming that the Leader size lies within a particular range $[\delta_{\min}, \delta_{\max}]$, which does not severely limit its possible size (the simulations used $[\delta/10, 10\delta]$).

A. Open-Loop Results

The (1)–(5) were implemented using a discrete extended Kalman filter with the addition of process noise to the model equations [34]. Using the original extended Kalman filter equations (1)–(3), the range is observable only during certain Follower maneuvers (typically oscillatory motion) so long as the Leader does not accelerate [1]. Beginning at randomly assigned locations within a ball of radius 25 ft around the origin for the follower and around the position (100, 0) for the leader, and with an initial range estimate lying in the interval [50, 150], the estimation process was simulated for 1000 instances with the follower undergoing oscillatory motion. At various points in the simulation the leader accelerates, decelerates, and/or engages in a turning maneuver (at times $t = 50, 80, 240$, and 300 s). The maneuvers are where the estimation algorithms go awry before resettling to steady state once the Leader resumes with a constant velocity. Correct measurement of ϵ and α requires knowledge of the camera parameters [35].

Fig. 6(a) depicts the estimation error arising from such a scenario. The Kalman filters are capable of tracking the correct range, however, it can be seen that the vision-based estimator has improved convergence properties relative to the bearings-

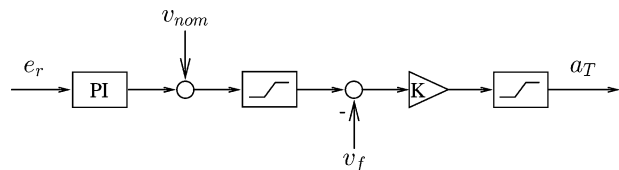


Fig. 7. Axial acceleration command control loop.

only estimator. The L_2 -norm of the estimation error was computed for the estimated range as a function of time for the two EKF models. Fig. 6(b) is a plot of the relative L_2 -norm error difference of the original EKF and the modified EKF as a percentage density; the relative error is the difference between the two L_2 -norm errors divided by the L_2 -norm error of the modified EKF. Median performance difference between the original EKF compared to the proposed EKF indicates 30% worse L_2 -error for the original EKF (the mean error was several orders of magnitude larger due to extreme outliers). In approximately 6% of the cases, the bearings-only EKF was not able to estimate the relative range and diverged.

IV. GUIDANCE AND CONTROL

This section provides an algorithm for tracking the Leader UV so as to move from estimation to feedback control. The algorithm is based on Proportional Navigation and LOS guidance laws [36]. Referring to the block diagram of Fig. 2, the Guidance block receives inputs from the Estimation block and two commands: the desired relative range r^* and the desired relative (lead) angle ϵ^* . The output of the algorithm are the acceleration commands to the inner control block of the UV. Control acceleration for the autonomous vehicle is decomposed into normal and tangential acceleration components a_N and a_T .

1) *Computation of a_N and a_T* : The purpose of the input a_N is to maintain the desired LOS angle between the Leader and Follower. Using the estimated values for the LOS and the LOS rate, define

$$a_N = nv_f (K_N \hat{x}_1 + (1 - K_N)e_\lambda) \quad (6)$$

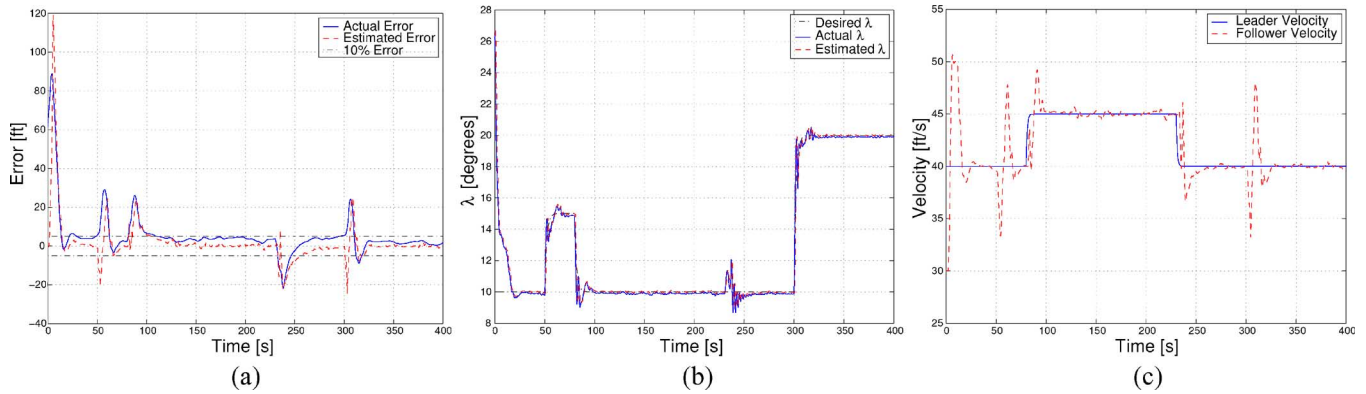


Fig. 8. Closed-loop Leader-Follower scenario. Changes in bearing (λ) or velocity denote a response to leader acceleration. (a) Range error versus time; (b) λ versus time; (c) follower velocity versus time.

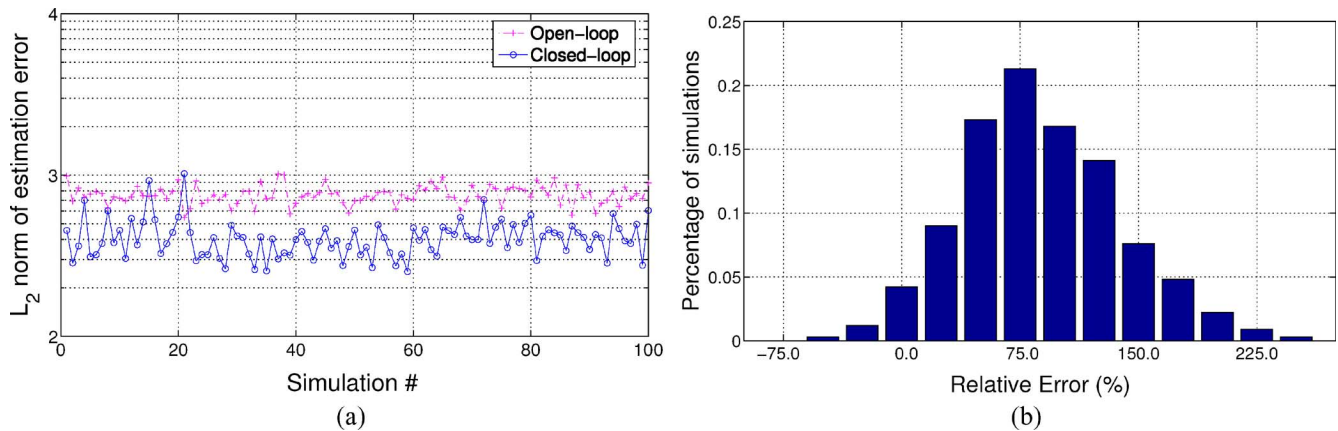


Fig. 9. Analysis of closed-loop performance of vision-based estimator. (a) Compares L_2 -norm error of the closed-loop vehicle tracking problem versus the open-loop estimation for the first 100 simulation runs. The two signals are not rigorously comparable since the vehicle was programmed to follow the correct trajectory in the open-loop problem. (b) Examines the relative error between the open- and closed-loop L_2 -norms for the 1000 simulations as a probability density. Open-loop estimation performance is expected to be approximately 90% worse than closed-loop performance on average.

where n is the proportional navigation constant, K_N is a parameter in the range $[0,1]$, v_f is the forward velocity of the Follower, and $e_\lambda \equiv \epsilon^* - (\theta_f - \hat{x}_3)$. The role of a_T is to track the desired relative range between the Leader and Follower. Consequently, a_T is a function of the range error $e_r = r^* - 1/\hat{x}_4$, described by the control loop depicted in Fig. 7, where v_{nom} is the nominal forward velocity of the Follower. The control loop also incorporates actuation limits.

The control commands were filtered during simulation to reproduce the dynamics of a vehicle with an autopilot. All simulations used the following transfer function realizations for the acceleration dynamics normal and tangent to the LOS

$$G_N(s) = \frac{9.9}{s^2 + 4.4s + 9.9}$$

$$G_T(s) = \frac{39.5}{s^2 + 8.8s + 39.5}$$

respectively.

A. Closed-Loop Results

By incorporating the guidance and control algorithms into the estimation process described in Section III, it is possible to

achieve the desired trajectory tracking goal of the Follower. Furthermore, the oscillatory trajectory required when performing bearings-only estimation is not needed in the closed-loop simulations. Under these conditions, the bearings-only estimator cannot achieve closed-loop vehicle tracking. Demonstrative simulation results of the closed-loop scenario with vision-based estimation are depicted in Fig. 8. As in the open-loop simulations, here the Leader maintains a steady velocity with occasional changes in bearing and/or speed. Leader accelerations induce disturbances in the estimation, which can be seen in Fig. 8(a). The visual processing and estimation algorithms work together to estimate the proper feedback for the guidance and control laws so that the Follower may track the Leader. The vision-based feedback rate was 2 Hz in order to account for processing time of the algorithm on nominal hardware. Fig. 9(a) depicts the open- and closed-loop L_2 -norm of the estimation error for 100 of the 1000 simulations performed. Comparing all of the simulations run, the open-loop estimation is expected to result in 90% worse L_2 -error performance on average. Strictly speaking, one should not compare the open-loop to the closed-loop performance, but lacking any additional reference, the open-loop data is the best available reference.

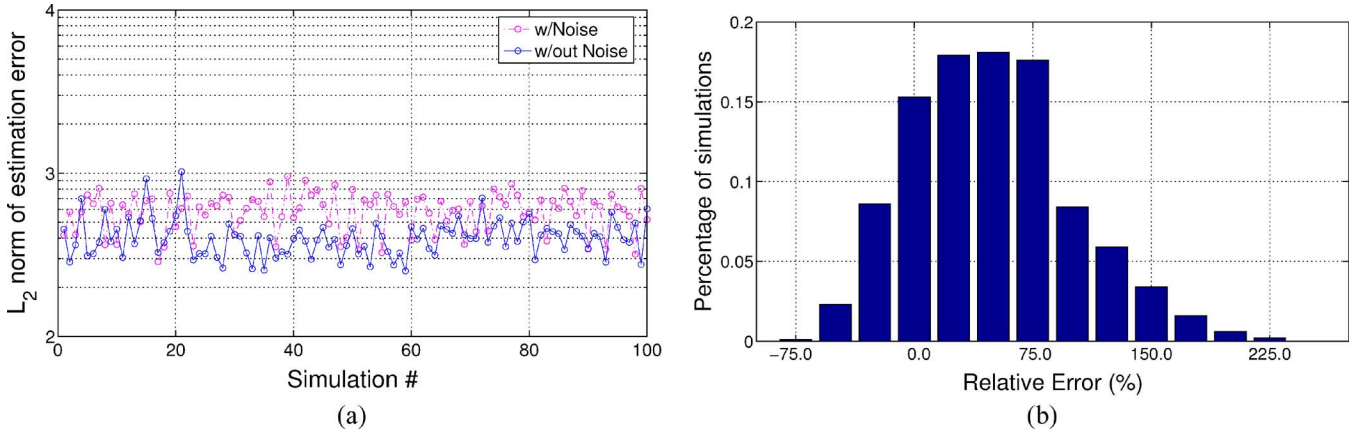


Fig. 10. Analysis of closed-loop performance of vision-based estimator with and without noise. (a) compares L_2 -norm error of the closed-loop vehicle tracking problem with noise and without noise. For the level of noise utilized, estimation performance is expected to be approximately 50% worse than closed-loop performance without noise on average. (a) L_2 -norm of estimation error; (b) relative error density of L_2 -norm errors.

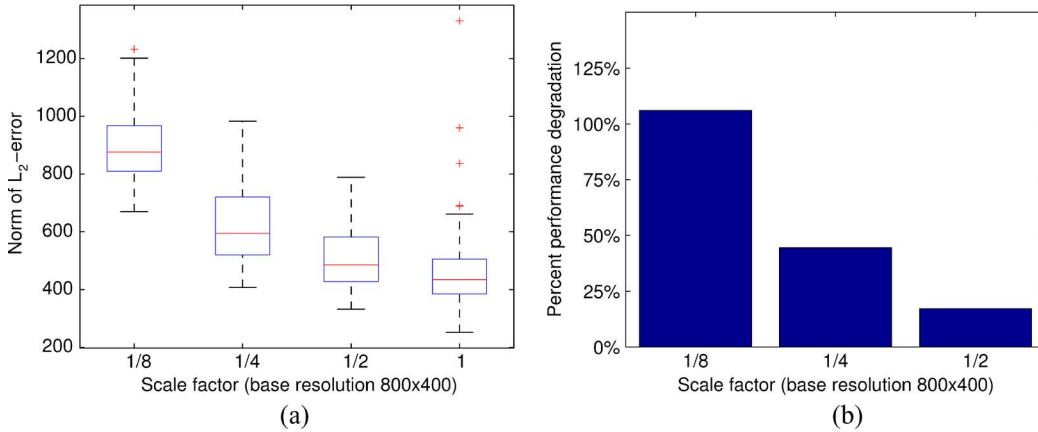


Fig. 11. Expected performance change when reducing the imaging sensor resolution. (a) Boxplot of estimation error L_2 -norm; (b) relative error versus baseline.

The estimation was also performed with Gaussian noise introduced into the measured follower dynamics. The standard deviations associated to the position estimates were $\sigma_x = 0.2$, $\sigma_y = 0.1$, and $\sigma_\theta = 1$, associated to the velocity estimates were $\sigma_{v_x} = 0.1$, $\sigma_{v_y} = 0.05$, and $\sigma_{v_\theta} = 2$, and associated to the acceleration estimates were $\sigma_{a_x} = 0.5$, $\sigma_{a_y} = 0.1$, and $\sigma_{a_\theta} = 4$, where the velocities and accelerations are with respect to body coordinates. The active contour measurements naturally have noise due to pixelization effects (and is present in all simulations). The noisy estimation is compared to the non-noisy estimation in Fig. 10. The uncertainty in the follower dynamics degraded the L_2 -error by approximately 50% percent on average. The expected L_2 -error per measurement for non-noisy estimation is 16 feet (within 10% error), whereas for noisy estimation it is 22 ft (slightly over 10% error).

In [12], Stein determines the expected error in their estimation algorithm based on the imaging sensor and its resolution. The resolution of the camera imposes limitations on the ability of the camera to resolve target geometry and motion. Fig. 11 illustrates the expected performance degradation when lowering the resolution of the imaging sensor. In Fig. 11(a) a boxplot of four different scenarios is given, describing the statistics arising from 100 simulations. Fig. 11(b) shows the mean percent change in estimation performance as the image resolution (baseline is 800

$\times 600$) is reduced up to a factor of eight. Significant degradation can be seen in the eight times reduction case; it is expected to perform approximately 100% worse than the baseline case. For eight times reduction with a target distance of 200 ft (the commanded following range), a one pixel error encodes for approximately 4 ft, which approaches 10% of the size of the Leader. A one pixel error also results in a range estimation error of about 20 ft, corresponding to 10% of the commanded distance. Equivalently, commanding a range eight times larger will result in the same level of uncertainty and one cannot achieve good tracking performance. As to be expected, the algorithm's effectiveness is range limited, where the imaging sensor and the target size determine the limiting range.

V. CONCLUSION AND FUTURE RESEARCH

The extended Kalman filter found in [1] was augmented by introducing additional image information available to vehicles with a fixed forward-pointing monocular camera. Active contours were used to track the follower in the image plane and provide the Kalman filter with the required input. Successful simulation of the proposed method has provided the proof-of-concept needed to continue investigation into real-time implementation of range estimation for automatic tracking of flying

vehicles. A full 3-D estimation strategy is needed for flying vehicles to track other flying vehicles. To achieve this, the filter state will have to incorporate the additional angle measurement found in the equivalent 3-D range estimation problem (using spherical coordinates) [16], [37]. Additional research should also go into reducing the sensitivity of the extended Kalman filter to target acceleration and into minimizing the convergence time and steady-state error of the estimator.

Adaptive estimation methods appear to be a promising avenue for dealing with these challenges [38], however, further investigation will be required to minimize the control cost of these methods. Once these objectives have been accomplished, the final step will be to integrate the vision-based range estimation strategy with the formation control algorithm of [3] on an experimental platform. Successful integration will provide us with a testbed to examine more complex vision-based navigation scenarios.

REFERENCES

- [1] V. J. Aidala and S. E. Hammel, "Utilization of modified polar coordinates for bearings-only tracking," *IEEE Trans. Autom. Control*, vol. 28, no. 3, pp. 283–294, Mar. 1983.
- [2] S. Avidan and A. Shashua, "Trajectory triangulation: 3D reconstruction of moving points from a monocular image sequence," *IEEE Trans. Pattern Anal. Mach. Intell.*, vol. 22, no. 4, pp. 348–357, Apr. 2000.
- [3] R. Sattigeri, A. J. Calise, and J. H. Evers, "An adaptive approach to vision-based formation control," presented at the AIAA GNC Conf., Austin, TX, 2003.
- [4] J. Barron, W. Ngai, and H. Spies, *Quantitative Depth Recovery From Time-Varying Optical Flow in a Kalman Filter Framework*, ser. Lecture Notes in Computer Science. New York: Springer-Verlag, 2003, pp. 346–355.
- [5] B. Sinoply, M. Micheli, G. Donato, and T. J. Koo, "Vision-based navigation for an unmanned aerial vehicle," in *Proc. IEEE Int. Conf. Robot. Autom.*, Korea, 2001, pp. 1757–1764.
- [6] H. Farid and E. Simoncelli, "Range estimation by optical differentiation," *J. Opt. Soc. Amer. A*, vol. 15, no. 7, pp. 1777–1786, 1998.
- [7] C. Harding and R. Lane, "Passive navigation from image sequences by use of a volumetric approach," *J. Opt. Soc. Amer. A*, vol. 19, no. 2, pp. 295–305, 2002.
- [8] A. Mitiche and S. Hadjres, "MDL estimation of a dense map of relative depth and 3D motion from a temporal sequence of images," *Pattern Anal. Appl.*, vol. 6, pp. 78–87, 2003.
- [9] O. Faugeras and R. Keriven, "Variational principles, surface evolution, PDEs, level set methods, and the stereo problem," *IEEE Trans. Image Process.*, vol. 7, no. 3, pp. 336–344, Mar. 1998.
- [10] M. Jankovic and B. Ghosh, "Visually guided ranging from observation of points, lines, and curves via an identifier based nonlinear observer," *Syst. Control Lett.*, vol. 25, pp. 63–73, 1995.
- [11] Y. Murphey, J. Chen, J. Crossman, J. Zhang, P. Richardson, and L. Sieh, "DepthFinder: A real-time depth detection system for aided driving," presented at the Int. Veh. Symp., Dearborn, MI, 2000.
- [12] G. Stein, O. Mano, and A. Shashua, "Vision-based ACC with a single camera: Bounds on range and range rate accuracy," presented at the Int. Veh. Symp., Columbus, OH, 2003.
- [13] A. Huster and S. Rock, "Relative position estimation for manipulation tasks by fusing vision and inertial measurements," in *Proc. MTS/IEEE Oceans Conf.*, Honolulu, HI, 2001, vol. 2, pp. 1025–1031.
- [14] E. Frew and S. Rock, "Trajectory generation for constant velocity target motion estimation using monocular vision," in *Proc. IEEE Int. Conf. Robot. Autom.*, 2003, pp. 3479–3484.
- [15] E. Frew, J. Langelaan, and S. Joo, "Adaptive receding horizon control for vision-based navigation of small unmanned aircraft," presented at the IEEE Amer. Control Conf., Boulder, CO, 2006.
- [16] R. Karlsson and F. Gustafsson, "Range estimation using angle-only target tracking with particle filters," in *Proc. IEEE Amer. Control Conf.*, 2001, pp. 3743–3748.
- [17] T. R. Kronhamn, "Angle-only tracking of maneuvering targets using adaptive-IMM multiple range models," in *Proc. RADAR*, 2002, pp. 310–314.
- [18] M. Moorman and T. Bullock, "A new estimator for passive tracking of maneuvering targets," in *Proc. IEEE Conf. Control Appl.*, 1992, vol. 2, pp. 1122–1127.
- [19] T. Vidal-Calleja, M. Bryson, S. Sukkarieh, A. Sanfeliu, and J. Andrade-Cetto, "On the observability of bearings-only SLAM," in *Proc. IEEE Int. Conf. Robot. Autom.*, 2007, pp. 4114–4119.
- [20] N. Kwok, Q. Ha, and G. Fang, "Data association in bearings-only SLAM using a cost function-based approach," in *Proc. IEEE Int. Conf. Robot. Autom.*, 2007, pp. 4108–4113.
- [21] A. De Luca, G. Oriolo, and P. Giordano, "On-line estimation of feature depth for image-based visual servoing," in *Proc. IEEE Int. Conf. Robot. Autom.*, 2007, pp. 2823–2828.
- [22] N. Cowan, O. Shakernia, R. Vidal, and S. Sastry, "Vision-based formation control," in *Proc. IEEE Int. Conf. Intell. Robot. Syst.*, 2003, pp. 1797–1801.
- [23] A. V. Das, R. Fierro, V. Kumar, J. P. Ostrowski, J. Speltzer, and C. J. Taylor, "A vision-based formation control framework," *IEEE Trans. Robot. Autom.*, vol. 18, no. 5, pp. 813–825, Oct. 2002.
- [24] G. Mariottini, G. Pappas, D. Prattichizzo, and K. Daniilidis, "Vision-based localization of leader-follower formations," in *Proc. IEEE Conf. Dec. Control*, 2005, pp. 635–640.
- [25] G. Mariottini, F. Morbidi, D. Prattichizzo, G. Pappas, and K. Daniilidis, "Leader-follower formations: Uncalibrated vision-based localization and control," in *Proc. IEEE Conf. Dec. Control*, 2005, pp. 2403–2408.
- [26] N. Moshtagh, A. Jadbabaie, and K. Daniilidis, "Vision-based control laws for distributed flocking of nonholonomic agents," in *Proc. IEEE Int. Conf. Robot. Autom.*, 2006, pp. 2769–2774.
- [27] S. Kichenassamy, A. Kumar, P. Olver, A. Tannenbaum, and A. Yezzi, "Conformal curvature flows: From phase transitions to active vision," *Archives for Rational Mechanics and Analysis*, vol. 134, pp. 275–301, 1996.
- [28] V. Caselles, R. Kimmel, and G. Sapiro, "Geodesic active contours," *Int. J. Computer Vision*, vol. 13, pp. 5–22, 1997.
- [29] M. Rousson and R. Deriche, "A variational framework for active and adaptive segmentation of vector valued images," presented at the IEEE Workshop Motion Video Comput., Orlando, FL, 2002.
- [30] S. J. Osher and J. A. Sethian, "Fronts propagation with curvature dependent speed: Algorithms based on Hamilton-Jacobi formulations," *J. Comp. Phys.*, vol. 79, pp. 12–49, 1988.
- [31] J. A. Sethian, "Curvature and the evolution of fronts," *Commun. Math. Phys.*, vol. 101, pp. 487–499, 1985.
- [32] A. Tannenbaum and A. Yezzi, *Visual Tracking, Active Vision, and Gradient Flows*, ser. Lecture Notes in Control and Information Science, G. Hager and D. Kriegman, Eds. New York: Springer-Verlag, 1998, vol. 237.
- [33] J. Helferty and D. Mudgett, "Optimal observer trajectories for bearings only tracking by minimizing the trace of the Cramer-Rao lower bound," in *Proc. IEEE Conf. Dec. Control*, 1993, pp. 936–939.
- [34] P. Zarchan and H. Mussof, "Fundamentals of Kalman filtering—A practical approach," in *Progress in Astronautics and Aeronautics*, P. Zarchan, Ed. Reston, VA: American Institution of Aerospace and Astronautical, Inc., 1998.
- [35] D. Forsyth and J. Ponce, *Computer Vision: A Modern Approach*. Englewood Cliffs, NJ: Prentice-Hall, 2003.
- [36] N. Shneydor, *Missile Guidance and Pursuit—Kinematics, Dynamics, and Control*. Chichester: Horwood, 1998.
- [37] C. Yang, C. Wang, L. C. J. J. J. Hung, and K. Fan, "Performance evaluation of range estimation via angle measurement," in *Proc. IPPR Conf. Comp. Vis., Graph., Image Process.*, 2003, pp. 242–249.
- [38] C. Cao and N. Hovakimyan, "Vision based air-to-air tracking using intelligent excitation," presented at the IEEE Amer. Control Conf., Boston, MA, 2005.